Spectrochimica Acta Part A: Molecular and Biomolecular Spectroscopy 173 (2016) 800–808

Contents lists available at ScienceDirect

Spectrochimica Acta Part A: Molecular and Biomolecular Spectroscopy

journal homepage: www.elsevier.com/locate/saa

Role of annealing on the structural and optical properties of nanostructured diaceto bis-benzimidazole Mn(II) complex thin films

P.A. Praveen[a], R. Ramesh Babu[a,*], K. Ramamurthi[b]

[a]Crystal Growth and Thin film Laboratory, Department of Physics, Bharathidasan University, Tiruchirappalli 620 024, Tamilnadu, India
[b]Crystal Growth and Thin film Laboratory, Department of Physics and Nanotechnology, SRM University, Kattankulathur 603 203, Kancheepuram, Tamilnadu, India

ARTICLE INFO

Article history:
Received 13 June 2016
Received in revised form 9 October 2016
Accepted 18 October 2016
Available online 20 October 2016

Keywords:
Metal organic thin films
Annealing
Nonlinear optical properties
Chemical bath deposition
CW Z-scan
Optical switching

ABSTRACT

A coordination complex, manganese incorporated benzimidazole, thin films were prepared by chemical bath deposition method. Structural characterization of the deposited films, carried out by Fourier transform infrared spectroscopy, Raman and electron paramagnetic resonance spectral analyses, reveals the distorted tetrahedral environment of the metal ion with bis-benzimidazole ligand. Further the molecular composition of the deposited metal complex was estimated by energy-dispersive X-ray spectroscopy. The prepared thin films were thermally treated to study the effect of annealing temperature on the surface morphology and the results showed that the surface homogeneity of the films increased for thermally treated films up to 150 °C. But distortion and voids were observed for the films annealed at 200 °C. The Raman analysis reveals the molecular hydrogen bond distortion which leads to the evaporation of the metal complex from the thin film surface with respect to annealing temperature. The linear and nonlinear optical properties of the as prepared and annealed films were studied using ultraviolet-visible transmittance spectroscopy, second harmonic generation and Z-scan analyses. Films annealed at 150 °C show a better linear transmittance in the visible region and larger SHG efficiency and third order nonlinear susceptibility when compared with the other samples. Further, the film annealed at 150 °C was subjected to optical switching analysis and demonstrated to have an inverted switching behavior.

1. Introduction

New materials with good nonlinear optical properties are in quest due to their extensive applications in photonics [1,2]. Different forms of materials such as crystals, thin films, polymer composites, glasses and nanoparticles are investigated in this regard. In which metal organic thin films gain much attention in the recent past due to their high physical and chemical stability compared to that of pure organic materials [1,3]. In addition, their ease of fabrication, fast response time and extensive design possibilities make these metal-organic thin film materials as an ideal candidate for waveguide fabrication and other photonic applications. In particular, many metal complexes have been investigated for optical switching and limiting applications and their two photon absorption, multiphoton absorption, excited state absorption, nonlinear refraction and nonlinear scattering mechanisms have also been studied [4,5]. In which, excited state absorption, a key mechanism in the *CW* region, could be used for optical limiting as well as optical switching purpose. Benzimidazole (BMZ), a heterocyclic aromatic molecule, and its derivatives are popular for their antifungal and antimicrobial activities [6]. In the last few decades they have attracted a considerable interest in different branches of material science and investigated for magnetic, anti-corrositivity, anti-cancer, photophysical and photochemical applications [7–9]. Especially many metal complexes of BMZ were used to model the complex biological systems. In this context, several crystallographic and spectroscopic analyses were performed on the metal complexes of BMZ [10–12]. BMZ is also a good nonlinear optical material with 4.5 times better SHG efficiency than the standard KDP crystal [13–16]. Recently third order nonlinear optical properties of BMZ and metal halide complexes of BMZ thin films were reported [3,17]. But the complexes with acetate substituents are expected to offer better hyperpolarizability values than the halide substituents [18]. Unfortunately, it is hard to find metal acetate based BMZ complexes in the literature. The reason is treating BMZ with metal acetate (M-OAc-BMZ) results rapid precipitation and the obtained products are often insoluble in most of

* Corresponding author.
E-mail address: rampap2k@yahoo.co.in (R. Babu).

http://dx.doi.org/10.1016/j.saa.2016.10.030
1386-1425/

the solvents. From the application point of view, homogeneous solid form is required to characterize and utilize the materials. Hence, in this work, manganese acetate based coordination complex of BMZ (Mn-BMZ) thin films were deposited for the first time. The choice of Mn is based on its potentiality towards third order optical nonlinearity [19]. Due to the solubility limitations of M-OAc-BMZ complexes and complexity of the physical methods, a simple chemical bath deposition method was used to deposit the films and the experimental parameters are adjusted to obtain a uniform thin solid layer on microscopic glass slides. The structural, linear transmittance, second harmonic generation efficiency and third order nonlinear susceptibility properties of the prepared samples are studied. Further, the role of surface morphology on the nonlinear optical properties are studied by annealing the films at different temperatures.

2. Experimental

All the chemicals used in the synthesis were analytical reagent grade and used without any further purification. For the deposition of Mn-BMZ films the ligand BMZ and manganese acetate tetrahydrate were taken in 2:1 ratio and dissolved separately using ethanol as the solvent. A few drops of acetic acid was added to the metal solution and then BMZ solution was added dropwise with stirring to the metal solution at room temperature. This solution was transformed to a refluxing container and the container was kept in a water bath. Two microscopic glass substrates were fused together by a sellotape and placed inside the solution container. The solution was refluxed for 5 h at 70 °C, whereupon the complex was deposited as thin film on the substrate. The thickness of the thin film can be altered by adjusting either the concentration or pH of the solution. In the present work, the concentration of the solution was fixed by choosing 0.1 M of BMZ (0.236 g) and 0.05 M of $(CH_3COO)_2$ $Mn.4H_2O$ (0.245 g) in 40 ml of ethanol. The pH of the solution can be varied by varying the amount of acetic acid added to the metal solution. No film formation was observed with an addition of acetic acid greater than 0.5 ml and also a rapid precipitation was evidenced in the case of addition of acetic acid less than 0.025 ml. After many trails, we adopted 0.2 ml of acetic acid (pH=8.06) as an optimized amount to deposit Mn-BMZ thin films. Supply of thermal energy increases the reaction rate between ligand and the metal acetate. Since, the rate of reaction is proportional to the temperature, concentration and pH, increase in any one of which or all would increase the number of Mn-BMZ molecules induced in the solution at a particular time. Often, if more number of molecules present in the solution they tend to precipitate at the bottom of the solution container. But at optimum temperature, concentration and pH, only a limited number of Mn-BMZ molecules induced in the solution and the molecules tend to nucleate on the surface of the substrates due to the higher surface energy of the substrate [20]. The formation of Mn-BMZ molecules can be evidenced from the change in color of the solution, from pale brown to dark brown. After 5 h the solution turns into turbid and then the substrates were removed from the solution. Shiny brown color thin film was observed on the substrate after the cleaning process with ethanol and double distilled water. In order to study the effect of annealing temperature, some of the as prepared samples (ASP) were annealed at 100 °C, 150 °C and 200 °C for 24 h and termed here as 100, 150 and 200 corresponding to their annealing temperature.

3. Instruments

The as deposited and annealed Mn-BMZ films were subjected to various structural and optical characterization studies. Surface topography of the thin films were studied using SEIKO SPA400-SPI4000 AFM unit in dynamic scanning mode with a scan speed of 0.5 Hz and the tip radius is about 10 nm. Crystallinity of the deposited thin films were analyzed by powder X-ray diffraction (PXRD) pattern using XPERT-PRO X-ray diffractometer. Compositional analysis was done by using Bruker energy-dispersive X-ray (EDS) spectrum with an operating voltage of 5 kV. The powder FT-IR (Perkin Elmer Spectrum RX I system) spectrum of the complex was recorded using the powders scratched from the film. Renishaw inVia Reflex Raman spectrometer was employed to record the Raman spectra of the samples. An Ar ion laser of wavelength 514.5 nm and spot size about 5 μm was used as the source and all the spectra were recorded in backscattering geometry. Transmittance spectrum of the samples were recorded using Perkin Elmer Lambda 35 UV-VIS spectrometer. The electron paramagnetic resonance (EPR) spectra of the complexes were recorded at room temperature in X-band frequency on a JEOL JES-FA200 EPR spectrometer. The microwave power is 1 mW and the modulation amplitude is about 160.00. The second harmonic generation of the samples was studied by placing the films normal to the probe beam of wavelength 1064 nm and the corresponding output at 532 nm was collected using a photomultiplier. Z-scan technique was used to calculate the nonlinear absorptive and refractive coefficients of the samples. A *CW* diode laser operated at 650 nm with the power of 20 mW was used as the source and the beam intensity was calculated about 7.8×10^8 W/cm^2. A lens of focal length 15 cm was used to focus the beam on the sample and the samples were scanned along the z-axis with respect to the direction of propagation of the laser beam. The variation in output intensity was measured in the far field and plotted. Optical path length is about 150 cm and the calculated Rayleigh length of the samples is about 9.8×10^{-2} m. Since, the thickness of the samples was less than the Rayleigh length, they could be treated as thin medium and this satisfies the critical condition $Z_R \gg L$ (where Z_R is the Rayleigh length and L is the sample thickness).

4. Results and Discussion

4.1. Structural Analysis

X-ray diffraction pattern (not shown) of the films showed a broad hump, which is a typical pattern of amorphous films. The FTIR spectrum of Mn-BMZ powder scratched from the thin film is shown in Fig. 1. Previous reports suggest that the vibrational spectrum of BMZ metal (M-BMZ) complexes almost resembles the benzimidazole spectrum except some specific metal-ligand absorption effects in the lower wavenumber region [21–24]. A small blue shift can be observed in the vibrational pattern of metal complexes with respect to BMZ spectrum. The amount of shift depends on the electrovalency of the incorporated metal ion. The upward shift observed in the Mn-BMZ spectrum can be attributed to the formation of metal complex. Further the presence of vibrational peak at far infrared region (~350 cm^{-1}) can be inferred as the evidence for metal-ligand (ν(M-L)) coordination. The presence of N-H vibrations in the region of 2700 cm^{-1} indicates that the N1 position of imidazolate ion

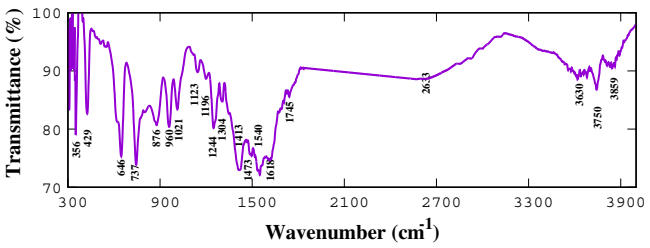

Fig. 1. FT-IR spectrum of Mn-BMZ complex.

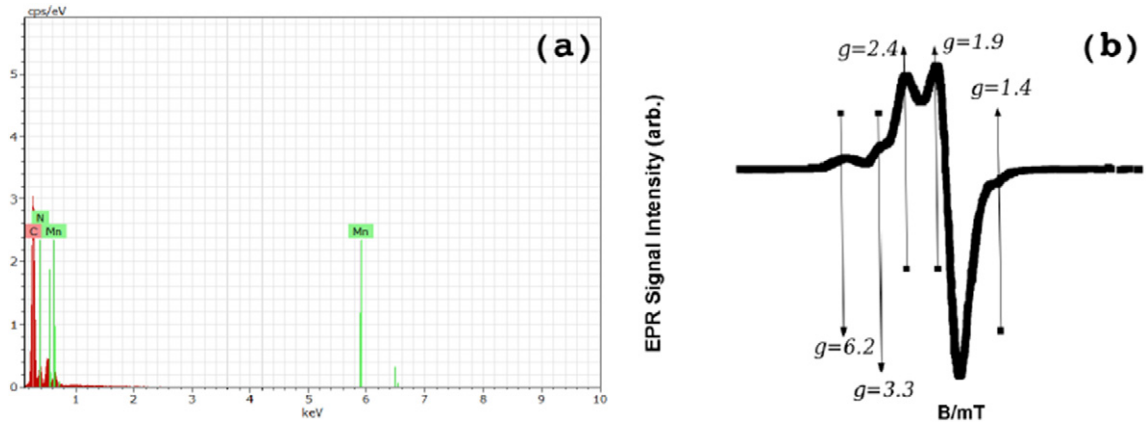

Fig. 2. (a) EDS and (b) EPR spectrum of Mn-BMZ complex.

remain unaffected and also confirms the formation of metal complex is through the N2 atom. Presence of absorption bands in the region 1500 cm^{-1} can be attributed to the influence of acetate ions [23]. Absorption bands in the region 3000 cm^{-1} are due to the solid state absorption of the samples (i.e., weak hydrogen bond formation between benzene rings) and the bands in the region of 3600–3800 cm^{-1} are attributed to the presence of water molecules in the complex [25]. Since it is hard to scratch the heat treated films, FTIR spectra of those were not recorded. The compositional analysis by energy-dispersive X-ray spectroscopy of the samples further confirms the incorporation of Mn ions in the BMZ medium (Fig. 2 (a)). The empirical formula derived from the EDS spectrum suggests bis form of BMZ with the metal ion. The powder EPR spectrum of Mn-BMZ complex (Fig. 2 (b)) recorded at room temperature exhibits hyperfine groups corresponding to monomeric manganese complex (Mn, I=5/2) with smaller zero field splitting energy [26,27]. Signal at g=2.4 is due to the transition from S=2 manifold, corresponding to $\Delta M_S = \pm 2$ transitions and signal at g=1.89 is due to the free Mn(II) ion. The signals from g=3.3 and 1.4 are due to two $\Delta M_S = \pm 1$ transitions arose from S=2 manifold. Low field signal observed at g=6.2 corresponds to S=1 manifold and they are only weakly allowed. The partially resolved structures at g=6.2 and g=3.3 can be attributed to the interaction between manganese and nitrogen which confirms the coordination of metal ion with benzimidazole ligand [26]. From the spectral and compositional analyses, the structure of Mn-BMZ complex was predicted as diaceto bis-benzimidazole Mn(II) and it is shown in Fig. 3. In order to confirm the same, the vibrational spectrum of the predicted complex was simulated using PM6 algorithm embedded in MOPAC2012 program [28]. The calculated values were scaled and fitted (Fig. 4) using the method reported elsewhere [29]. The calculated values are in good agreement with the observed frequencies and the percentage of error is approximated about less than 2%.

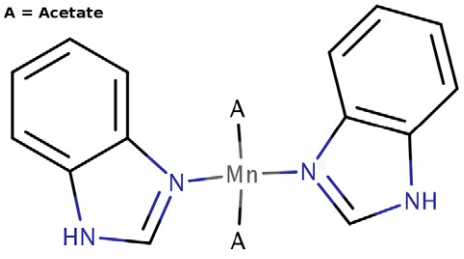

Fig. 3. Predicted structure of the Mn-BMZ complex.

4.2. Surface Analysis

Surface morphology of the thin films plays a vital role in the linear and nonlinear optical properties. The atomic force microscopy (AFM) images of the as prepared and annealed Mn-BMZ samples are shown in Fig. 5 and the corresponding grain size, root mean square roughness (R_q), skewness (R_sk) and kurtosis (R_ku) values are given in Table 1. It is a well known fact that the diffusion coefficient exponentially increases with temperature. Thus the increase in surface homogeneity of the films with increasing annealing temperature can be interpreted to surface diffusion [30]. This can be further evidenced from the R_q values given in Table 1. The decrease in R_q values, for the films annealed at 100 and 150 °C corresponds to the increase in homogeneity of the film surface. Also the decrement in R_sk values of these films reveals the surface with more planar and predominant by the valleys. Further R_ku values showed that the platykurtic nature of the films increases for the films annealed at 100 and 150 °C. But the dramatic change in the surface parameters observed for the films annealed at 200 °C is due to the surface distortion of the films.

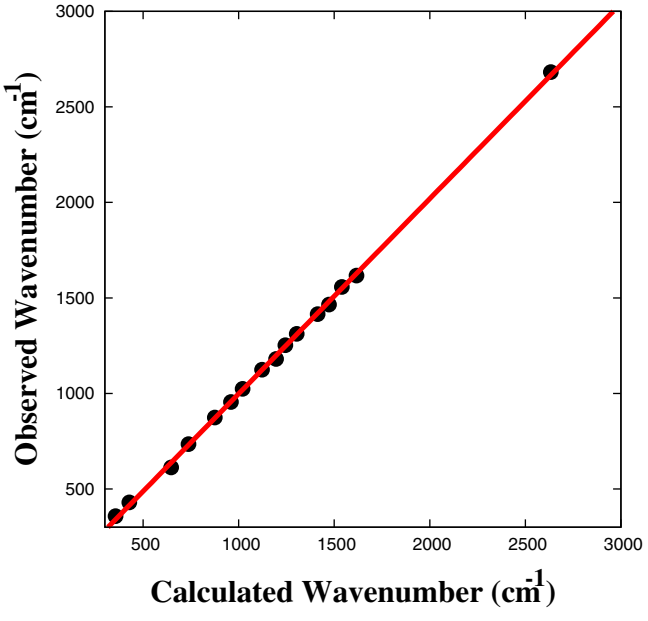

Fig. 4. Fitted values of observed and calculated frequencies.

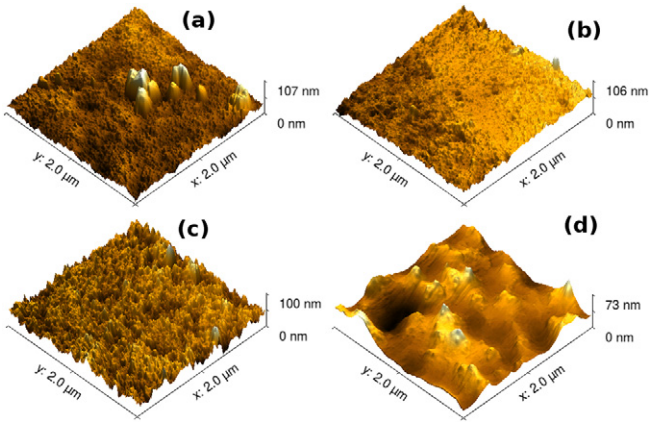

Fig. 5. Surface morphology of Mn-BMZ thin films: (a) As prepared, and annealed at (b) 100 °C, (c) 150 °C, and (d) 200 °C.

Table 1
Calculated surface parameters of Mn-BMZ thin films.

Sample	Grain size (nm^2)	RMS roughness (R_q) (nm)	Skewness (R_sk) (arb.)	Kurtosis (R_ku)(arb.)
ASP	40.96	10.77	2.34	8.2
100	29.07	5.69	−0.03	2.5
150	28.03	5.56	0.22	0.64
200	80.64	11.8	3.43	28.1

The molecular distortion at surface may either due to the evaporation of the molecules from the surface or due to the decomposition of the molecules. This can be investigated by analyzing the molecular composition of Mn-BMZ by EDS and Raman studies. At higher temperatures, even though there is a reduction in the overall weight percentage of the molecules, the composition of the samples remains almost invariable. This shows that there is no molecular decomposition of the material at higher temperatures. Fig. 6 shows the Raman spectrum of as prepared and the samples annealed at 100, 150 and 200 °C. From the Raman spectrum, peaks at 321, 379 cm^{-1} (correspond to the C–H solid state bonding) and 659 cm^{-1} (corresponds to out plane modes of C–H bond of BMZ) are missing in the samples annealed at 200 °C. This can be explained by the fact that the organic materials solidify by forming weak hydrogen bonds between the molecules. BMZ is also form such a weak bond by means of four C–H bonds. Due to the breaking of these bonds (Fig. 7) distortion of film surface was observed [31].

4.3. Linear Optical Properties

Transmittance spectrum of Mn-BMZ complex thin films was studied by UV-Vis. spectrum analysis and is shown in Fig. 8. A broad absorption peak is observed in the region between 300 nm and 500 nm for all the films. At higher wavelength region, the films show high optical transmission about 80% and this ensures the optical

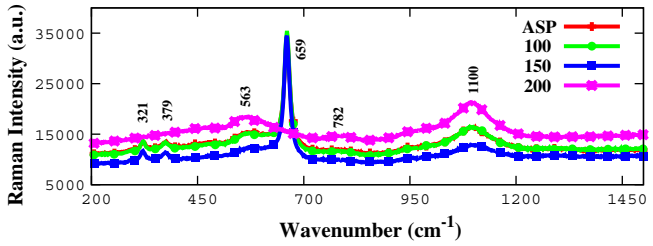

Fig. 6. Raman spectrum of Mn-BMZ thin films.

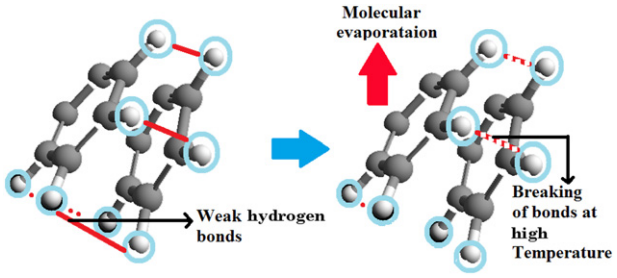

Fig. 7. H-bond breaking in the benzene ring of solid BMZ molecule.

homogeneity of the deposited films. The absorption maxima centered around 320–350 nm can be assigned to $\pi-\pi^*$ interligand transmissions and the secondary peak observed around 500 nm can be inferred to the metal to ligand charge transfer $d\pi_{(Mn)}-\pi^*_{(ligand)}$ transition [23]. The enhancement in transmission percentage of annealed films with respect to their annealing temperature can be interpreted to the variation in grain size. It is a well known fact that the transmission percentage of thin films increases with decrease in grain size [17]. A similar phenomena is observed in the case of Mn-BMZ films too. Increase in grain size at 200 °C of annealing temperature results lower transmission in the sample. The red shift in the absorption maxima indicates the possibility of electronic transition in lower energy region with respect to the decrement in grain size.

4.4. Nonlinear Optical Properties

4.4.1. Second Harmonic Generation Efficiency

Second harmonic generation (SHG) efficiency of the Mn-BMZ films was measured using a modified Kurtz-Perry method and the schematic of the setup is shown in Fig. 9. Measurements were carried out using a Q-switched Nd:YAG laser (Quanta-Ray DCR-11 Model) of operating wavelength 1064 nm, power of 190 mJ and the pulse width of 10 ns. The amplitude of SHG in the films was measured by placing the films normal to the probe beam [32] and the second harmonic generation in the samples was confirmed by the observation of green radiation. The output amplitude usually increases with increase in the input energy and it may diminish if some damage occurs to the sample. In the case of Mn-BMZ samples, up to 25 mJ the output increases with respect to input energy and then it begins to decreases. So, we have chosen 25 mJ as operating laser power for all the SHG measurements. Initially, the beam was allowed to pass between two IR reflectors and then on to the sample. The output

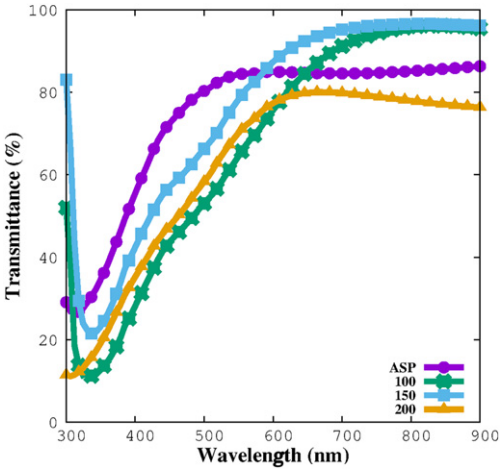

Fig. 8. Transmission spectrum of Mn-BMZ samples.

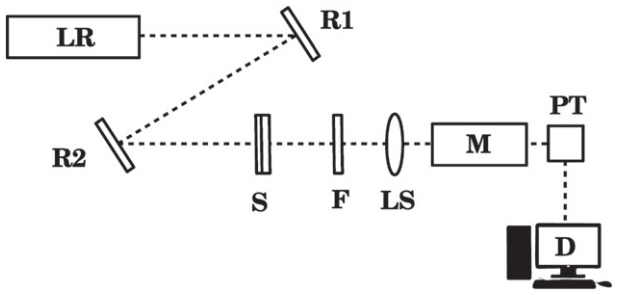

Fig. 9. Experimental setup used to measure SHG in Mn-BMZ samples, where LR is the Q-switched Nd:YAG laser, R1 and R2 are IR reflectors, S is the sample, F is the IR filter, LS is the focusing lens, M is the monochromator, PT is the photomultiplier and D is the data acquisition system.

from the sample was filtered by using an IR filter and focused on to the monochromator using a focusing lens. Then the output from the monochromator was collected by using a photomultiplier and the data was collected using a computer. The relative SHG efficiency of the films was calculated by the ratio between the intensity counts of Mn-BMZ and BMZ thin films of similar thickness and the calculated values are shown in Table 2. The variation in SHG efficiency of the Mn-BMZ samples with respect to annealing temperature can be attributed to the variation in surface homogeneity (Fig. 5). During the deposition of Mn-BMZ thin films, due to the dipolar forces the molecules tend to align in the antiparallel fashion. Upon annealing, molecular orientation aligned and this improves the SHG efficiency in the films [33]. In the case of organic/metal organic materials, major contribution is expected to arise from the molecules rather than their molecular arrangement. This is the reason that even the strong surface distortion at 200 °C of annealing temperature slightly reduced the SHG efficiency.

4.4.2. Third Order Optical Nonlinearity

The nonlinear absorptive effects of the samples were studied using open aperture Z-scan curves (Fig. 10). All the films, excluding the films annealed at 200 °C, show saturable absorption (SA) whereas the film annealed 200 °C shows reverse saturable absorption (RSA) characteristics. The SA and RSA behavior of the films can be inferred with the help of five-level electronic transition model [34,35]. Let us consider two sets of energy levels S_n and T_n (n=1, 2, 3 . . .) corresponding to the singlet and triplet states of a molecule, respectively. Often, when the sample is irradiated by a laser source, molecules in the ground state (S_0) get excited to the first electronic excited state (S_1), upon continuous laser irradiation they can further make a transition to the second excited state (S_2) or to the first triplet state (T_1) by intersystem crossing (ISC). This type of transitions are referred as excited state absorption (ESA). If the excited state absorption cross section (σ_{ex}) is greater than that of the ground state absorption cross section (σ_0) then RSA will takes place. On the other hand, if σ_0 is greater than σ_{ex}, saturable absorption will be observed [34]. The observation of SA in Mn-BMZ films suggests that the ESA has lower excited state absorption cross section than that of the ground state absorption cross section and $S_1 \rightarrow S_2$ transition process might dominate in the electronic transitions. In the open aperture Z-scan, the

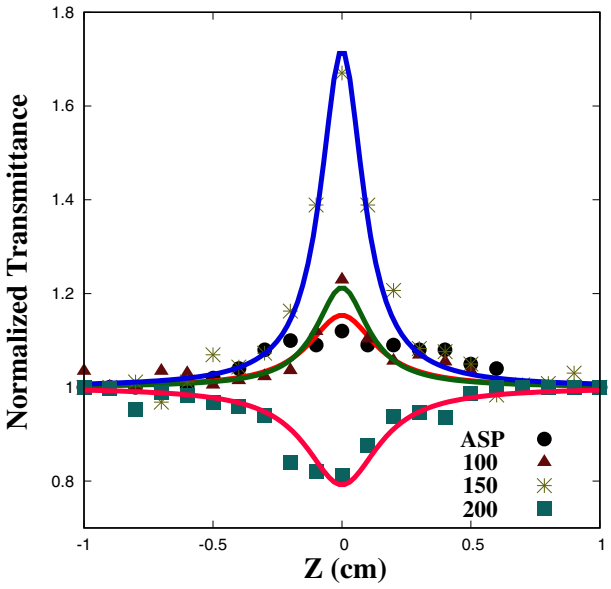

Fig. 10. OA Z-scan curves of Mn-BMZ films.

absorption coefficient of the films can be related to transmittance using the relation,

$$T(Z) = 1 - \frac{q_0}{2\sqrt{2}\left(1 + \frac{z^2}{z_0^2}\right)} \quad (1)$$

where,

$$q_0 = \beta I_0 L_{eff} \quad (2)$$

I_0 is the intensity of the laser beam at focus (z=0), L_{eff} is the effective thickness of the sample and it can be calculated by using the relation,

$$L_{eff} = \frac{1 - e^{\alpha L}}{\alpha} \quad (3)$$

here L is the thickness of the films and α is the linear absorption coefficient of thin films and z_0 is the Rayleigh radius, could be obtained from the relation $z_0 = \pi\omega_0^2/\lambda$, where ω_0 is the beam waist and λ is the wavelength of source. The q_0 value was obtained by fitting the Eq. (1) to the experimental data and the β value was calculated by substituting back q_0 values in Eq. (2). The nonlinear refractive effects of the samples were measured using closed aperture (CA) Z-scan configuration. An aperture with linear transmittance 0.4 was placed in front of the detector and the variation of transmittance was measured for different sample positions. The obtained plots imitate the open aperture Z-scan curves. In order to extract the nonlinear refractive effects, closed aperture data was divided by open aperture data and the corresponding graphs are shown in Fig. 11. The

Table 2
SHG efficiency and Third order nonlinear optical properties of Mn-BMZ films.

Sample	SHG efficiency	β (m/W)	$n_2 \times 10^{-7}$ (m^2/W)	$\chi^{(3)} \times 10^{-9}$ esu	FOM $\times 10^{-14}$ esu
ASP	2.37	−0.41	−1.57	2.77	1.10
100	2.54	−0.52	−1.60	3.00	1.17
150	2.67	−1.95	−2.16	3.93	1.47
200	2.51	1.22	5.40	1.64	0.30

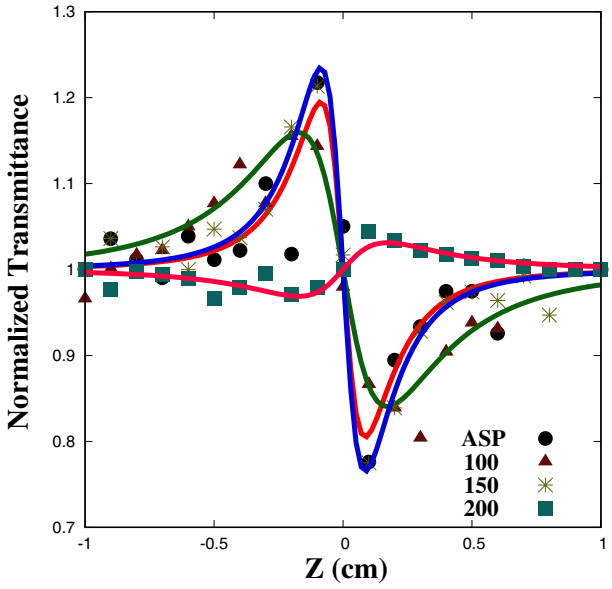

Fig. 11. CA Z-scan curves of Mn-BMZ films.

theoretical relation between transmittance as a function of distance can be expressed as [34],

$$T(Z) = 1 - \frac{4\Delta\Phi.x}{(x^2+9)(x^2+1)} \tag{4}$$

where x=z/z_0, $\Delta\Phi$ is the laser induced phase shift and related to the nonlinear refractive index by the equation

$$n_2 = \frac{\Delta\Phi\lambda\alpha}{2\pi I_0(1-e^{-\alpha l})} \tag{5}$$

Eq. (4) is fitted to the experimental data to obtain $\Delta\Phi$ and by substituting back the value of $\Delta\Phi$ in Eq. (5), the n_2 value was calculated. Since the *CW* laser is used as the source, origin of nonlinear refractivity can be attributed to thermal effects [3]. The calculated values of nonlinear optical properties are given in Table 2.

The nonlinear absorption and refractive coefficients are used to calculate the real and imaginary part of third order nonlinear susceptibility [36].

$$Im\chi^{(3)} = \frac{n^2\epsilon_0 C\lambda\beta}{2\pi} \tag{6}$$

and

$$Re\chi^{(3)} = 2n^2\epsilon_0 C n_2 \tag{7}$$

where C is the speed of light in vacuum, ϵ_0 is the free space permittivity and n is the linear refractive index of the material. The absolute values of third order nonlinear susceptibilities of Mn-BMZ films were calculated using the relation,

$$\left|\chi^{(3)}\right| = \left[\left(Re\chi^{(3)}\right)^2 + \left(Im\chi^{(3)}\right)^2\right]^{1/2} \tag{8}$$

Table 2 provides the calculated third order nonlinear optical parameters of Mn-BMZ thin films. The origin of observed third order nonlinearities is due to thermal effects. When the *CW* laser beam traversed through the sample, it has been absorbed by the sample by linear absorption. Often, absorption of high energy beam creates a heating effect in the medium, which induces a local thermal gradient. Induction of thermal gradient alters the refractivity of the medium, which acts as lens, known as thermal lens. Further propagation of the beam through this lens alter the phase of the propagating beam and thus induces the nonlinear effects. In Z-scan analysis, it is well established that the peak-valley separation in CA scan about 1.7 times of Rayleigh range indicates Kerr-type nonlinearity. More than that could be attributed to the thermal effects [37]. Since, the peak-valley separation in our case is around 2.8 times of Z_0, supports the discussion above. Further, the calculated nonlinear absorptive and refractive coefficients are compared with the previous reports and given in Table 3. It should be kept in mind that depending on the nature of the medium, laser source, power, sample thickness, sample dimension (crystals/films/particles) etc., the observed nonlinear parameters may vary. Given comparison is meant to provide an idea about β and n_2 of different materials of different forms. In order to estimate the potentiality of the different Mn-BMZ samples, figure of merit (FOM) was calculated using the relation χ^3/α. Higher the FOM, higher would be the sample's third order optical nonlinearity. With better linear transmittance and higher nonlinear absorption coefficient, sample annealed at 150 °C shows higher FOM.

5. Role of Surface Morphology on Optical Properties

The variation in optical properties with respect to the surface morphology (especially in the case of the sample annealed at 200 °C) can be explained in terms of molecular deformation process. In any metal organic thin films, the molecular packing in a layer can be expressed in terms of rotation (θ) and bending (ϕ) angles of a molecule in that particular plane. Upon annealing, due to thermal diffusion, the molecules tend to reorient themselves (i.e., θ and ϕ

Table 3
Comparison of the measured values of β and n_2 of Mn-BMZ with the previous reports.

Sample	Medium	CW source (nm)	Power (mW)	β (cm/W)	n_2 (cm^2/W)	Reference
Mn-BMZ	–	650	20	-0.41×10^{-2}	-1.57×10^{-11}	This work
Tetra tert-butyl phthalocynanine	PMMA	633	14	−0.49	-12.0×10^{-6}	[37]
Zinc tetra tert-butyl phthalocynanine	PMMA	633	14	−1.1	-14.2×10^{-6}	[37]
Graphene oxide	Ethylene glycol	532	50	6.1×10^{-3}	4.0×10^{-8}	[38]
$ZnFe_2O_4$	Ethylene glycol	532	50	6.1×10^{-3}	3.0×10^{-8}	[38]
Thiobarbituric acid derivative T1	Chloroform	632.8	10	-0.890×10^{-3}	-0.424×10^{-7}	[39]
Thiobarbituric acid derivative T2	Chloroform	632.8	10	1.667×10^{-3}	-1.571×10^{-7}	[39]
15-DAAQ	PMMA	532	–	7.88×10^{-5}	-3.13×10^{-15}	[40]
Pyran dye	PMMA	514	–	8.37×10^{-5}	0.66×10^{-9}	[41]
TiO_2 nanocomposites	Ethylene glycol	632.8	50	0.337×10^{-7}	-0.43×10^{-14}	[42]
Au/TiO_2 nanocomposites	Ethylene glycol	632.8	50	0.2×10^{-7}	-0.565×10^{-14}	[42]
PVP/TiO_2 nano-fibers	–	632.8	–	2×10^{-3}	-1.01×10^{-7}	[43]
Ni nanoparticles	Ethanol	632.8	48	0.79×10^{-3}	-3.04×10^{-7}	[44]

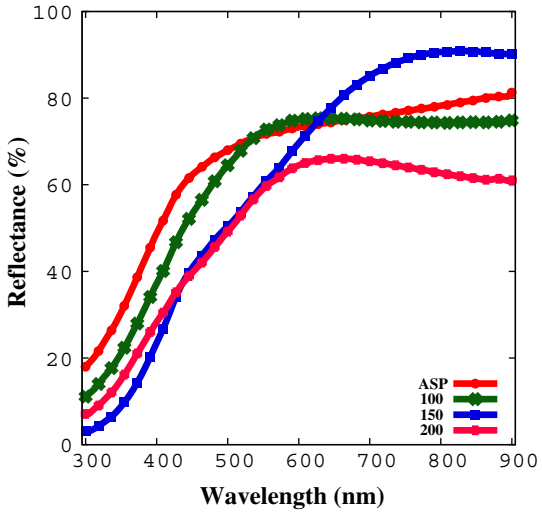

Fig. 12. Reflectance spectrum of Mn-BMZ samples.

values changes). During such a process, two phenomenon will take place. The dislocation densities of the sample will be reduced and depending upon the molecular weight, deformation of molecules with respect to annealing temperature will takes place [45]. These variations can significantly affects the physical properties, in particular, the optical properties [46]. In the case of Mn-BMZ films, the strong molecular deformations at 200 °C of annealing temperature can cause the unfilled d-valence orbital, formed due to the interaction between π electrons of the ligand and d-shell electrons of the metal ion, to split into several levels. This in turn will increase the optical absorption in the samples. It is worth to note that higher the grain size, lower would be the coherence between the molecular networks [47]. This explains the variation of optical properties of the sample annealed at 200 °C with respect to its (increased) grain size. On the other hand, since the SHG efficiency of the samples entirely depends on the d-shell of the Mn ion in the molecular structure, only slight variation in SHG efficiency with respect to surface scattering has been observed, similar to the effects observed in porphyrine and phthalocyanine molecules [48]. But, in order to precisely explore the surface dynamics, combined experimental and theoretical studies such as scanning tunnelling microscope analysis and density functional theory/molecular dynamics simulations are required. We hope such a studies will be reported as our future work. The observed switch over phenomena from SA to RSA and self defocusing to self focusing in the sample annealed at 200 °C can be accounted to the variation in input intensity with respect to the reflectivity of the samples. Switch over phenomena are often observed with pulsed laser sources and two or three photon absorption could be the possible mechanism for such a behavior. It is rare to observe a switch over phenomena with a *CW* pump since with a *CW* laser it is not possible to produce an intensity about 10^8 W/cm^2, which is the minimum requirement to observe the above mentioned effects. Even the available reports on switch over behavior in a *CW* regime, mainly studied in a solution form or doped in polymers and the effect is attributed to the aggregation of particles in the solution/polymer, with respect to their concentration [49]. But, in our case the variation in the input intensity with respect to the surface morphology can be attributed to the observed effect. Because, in nonlinear optical materials, switch over from one phenomena to other phenomena can arise if the input intensity crosses the threshold value, say I_c. So, by varying the input intensity on the sample one could vary the nonlinear optical phenomena. In the Z-scan experiment, the intensity of the light traversed through the sample can varies by means two factors: (i) depending on the position of the sample with respect to the focusing lens and (ii) by the amount of surface reflections on the sample. Higher the reflectivity of the sample, lower would be the light traversed through the sample. In the case of high reflectance samples like Mn-BMZ, variation in surface morphology would alters the reflectivity of the sample. For the samples annealed at 200 °C, decrease in reflectance (Fig. 12) should increase the input intensity which crosses above I_c results the observed phenomena, similar to the report by Chen Dai-Jian et al. [50]. This is possible in the case of organometallics and polymers even in the *CW* regime since the saturation intensities are very low for these systems (about 10^4 W/cm^2) [49].

6. Optical Switching

The thermal assisted nonlinear phenomena can be effectively utilized for optical switching applications. The inverted switching behavior of Mn-BMZ films annealed at 150 °C was studied. The principle is that the population dynamics of the sample vary with respect to the intensity of the incident laser. i.e., a high power laser can produce a strong heating effect in a nonlinear medium than a low power laser and the corresponding variation in the excitation dynamics can alter the nonlinear effects [51]. Fig. 13 shows the schematic of an optical switching experimental setup. A *CW* diode laser of power 20 mW was used as the pump (writing) beam and a weak laser of power 1 mW was used as the probe (reading) beam. Both the lasers were operated at the wavelength of 650 nm. Since the sample possesses very low absorption in the 650 nm region, any observed variation can be attributed to the effect of thermal nonlinearity. The pump beam was passed through a mechanical chopper in order to obtain a square wave pattern (ON/OFF states). A lens of focal length 6 cm was used to focus the beams on the sample and the variation in probe beam with respect to the pump beam was measured using an oscilloscope. The obtained traces are shown in Fig. 14. By properly adjusting the revolutions per minute (RPM) of the mechanical chopper, a frequency variation up to 1 kHz can be achieved. When the pump beam is in OFF state, the low power probe beam does

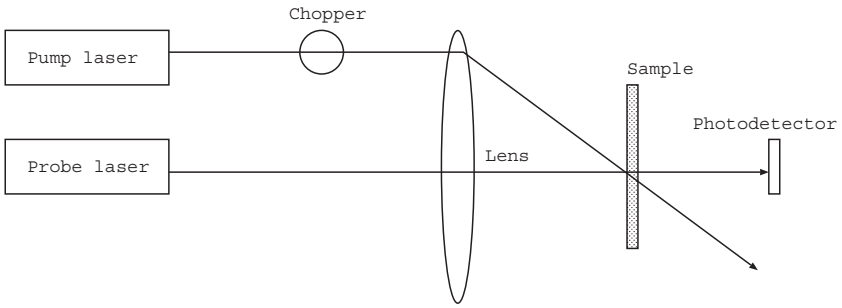

Fig. 13. Schematic of an optical switching setup.

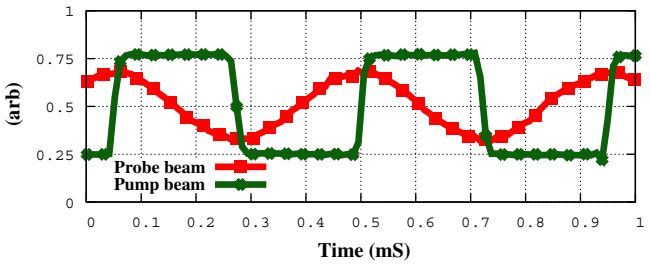

Fig. 14. Demonstration of optical inverter switch in Mn-BMZ film annealed at 150 °C.

not induce much effect in the nonlinear medium and it transmits through the sample as it is. But when the pump beam is in ON state, the intensity of the beam induces the thermal assisted nonlinear effects in the medium which leads to the saturation of population in the excited state and correspondingly a low state was obtained as output. This corresponds to the inverted switching behavior of NOT gate, analogous to electronics.

7. Conclusions

Manganese incorporated benzimidazole metal complex thin films were deposited by chemical deposition method and the XRD studies revealed the amorphous nature of the deposited samples. Presence of metal ligand vibrations at 350 cm^{-1} and the observation of N-H and C-H vibrations at 3100–3400 cm^{-1} confirms the formation of Mn-BMZ complex by the coordination of Mn through N2 atom of the imidazole ring. Further, the distorted tetrahedral environment of metal ion with benzimidazole ligand was confirmed by EPR analysis and the molecular composition was estimated using EDS analysis. AFM studies showed that the surface homogeneity of the samples varies with respect to the annealing temperature. Even though, annealing induced a positive impact on the surface homogeneity, surface distortion and voids were observed on the films annealed at 200 °C due to the molecular evaporation. The breaking of hydrogen bonds with respect to the annealing temperature leads to the rapid molecular evaporation at 200 °C and which was studied through Raman analysis. For the films annealed at 100 and 150 °C, decrease in grain size increases the optical transmission percentage. Similarly annealing induced molecular alignment improves the SHG efficiency of the samples annealed at 100 and 150 °C. On the other hand optical scattering loss due to surface distortion reduces the performance and a corresponding decrement in optical transmittance and SHG efficiency was observed for the sample annealed at 200 °C. In the case of third order nonlinear studies ASP sample and the samples annealed at 100 and 150 °C show a self-defocusing effect (CA curves) and saturable absorption (OA curves) in the Z-scan analysis. But the film annealed at 200 °C shows an switch over phenomena from SA to RSA in OA curves and defocusing to focusing in CA curves due to the variation in input intensity with respect to the surface defects. Calculated third order nonlinear susceptibility of the samples was ~1.64 to 3.93 $\times 10^{-9}$ esu and the films annealed at 150 °C showed better FOM than the as prepared and other annealed samples. Inverted switching behavior is demonstrated in one of the fabricated films and thermal assisted nonlinearity can be attributed to the switching effect in samples. The major advantage of these type of switches is their low linear absorption in the operation wavelength and low pumping power requirement. This ensures the compactness and cost effective in device fabrication.

Acknowledgments

The authors acknowledge the financial assistance from the School of Physics, provided by DST-FIST (Order No.: SR/FIST/PSI-204/2015 (c)) for the establishment of some laboratory utensils. Further, P.A. Praveen thank the UGC-BSR Govt. of India for financial assistance in the form of 'Research Fellowship in Science for Meritorious Students' (F.4-1/2006/7-197/2007(BSR)).

References

[1] P.G. Lacroix, I. Malfant, C. Lepetit, Second-order nonlinear optics in coordination chemistry: an open door towards multi-functional materials and molecular switches, Coord. Chem. Rev. 308 (2016) 381–394.
[2] H. Harutyunyan, Nonlinear optics: anti-diffraction of light, Nat. Photonics 9 (4) (2015) 213–214.
[3] P.A. Praveen, R. Ramesh Babu, K. Jothivenkatachalam, K. Ramamurthi, Spectral, morphological, linear and nonlinear optical properties of nanostructured benzimidazole metal complex thin films, Spectrochim. Acta A Mol. Biomol. Spectrosc. 150 (2015) 280–289.
[4] G. Lu, J. Li, S. Yan, C. He, M. Shi, W. Zhu, Z. Ou, K.M. Kadish, Self-assembled organic nanostructures and nonlinear optical properties of heteroleptic corrole-phthalocyanine europium triple-decker complexes, Dyes Pigments 121 (2015) 38–45.
[5] S.O. Sanusi, E. Antunes, T. Nyokong, Nonlinear optical behavior of metal octaphenoxy phthalocyanines: effect of distortion caused by the central metal, J. Porphyrins Phthalocyanines 17 (10) (2013) 920–927.
[6] S. Khabnadideh, Z. Rezaei, K. Pakshir, K. Zomorodian, N. Ghafari, Synthesis and antifungal activity of benzimidazole, benzotriazole and aminothiazole derivatives, Res. Pharm. Sci. 7 (2) (2012) 65.
[7] H.J. Kim, C.H. Heo, H.M. Kim, Benzimidazole-based ratiometric two-photon fluorescent probes for acidic pH in live cells and tissues, J. Am. Chem. Soc. 135 (47) (2013) 17969–17977.
[8] Y. Tang, F. Zhang, S. Hu, Z. Cao, Z. Wu, W. Jing, Novel benzimidazole derivatives as corrosion inhibitors of mild steel in the acidic media. Part I: gravimetric, electrochemical, SEM and XPS studies, Corros. Sci. 74 (2013) 271–282.
[9] B. Pan, B. Wang, Y. Wang, P. Xu, L. Wang, J. Chen, D. Ma, A simple carbazole-N-benzimidazole bipolar host material for highly efficient blue and single layer white phosphorescent organic light-emitting diodes, J. Mater. Chem. C 2 (14) (2014) 2466–2469.
[10] A. Ashraf, W.A. Siddiqui, J. Akbar, G. Mustafa, H. Krautscheid, N. Ullah, B. Mirza, F. Sher, M. Hanif, C.G. Hartinger, Metal complexes of benzimidazole derived sulfonamide: synthesis, molecular structures and antimicrobial activity, Inorg. Chim. Acta 443 (2016) 179–185.
[11] N.A. Mazlan, T.B.S. Ravoof, E.R. Tiekink, M.I.M. Tahir, A. Veerakumarasivam, K.A. Crouse, Mixed-ligand metal complexes containing an ONS Schiff base and imidazole/benzimidazole ligands: synthesis, characterization, crystallography and biological activity, Transit. Met. Chem. 39 (6) (2014) 633–639.
[12] M.U. Rehman, M. Arif, M. Imran, M. Farooq, Synthesis, Characterization and antimicrobial properties of Mannich base cyclization derivatives of benzimidazole and their metal complexes, Am. J. Chem. 4 (1) (2014) 10–21.
[13] N. Vijayan, G. Bhagavannarayana, S. Halder, S. Verma, J. Philip, R. Philip, B. Rathi, X-ray topography, photopyroelectric and two-photon absorption studies on solution grown benzimidazole single crystal, Appl. Phys. A 110 (1) (2013) 55–58.
[14] R. Bright, M.K.R. Rahman, M. Shkir, N. Vijayan, D. Sajan, M.M. Abdullah, G. Bhagavannarayana, M.A. Wahab, Growth, optical, mechanical, thermal and second harmonic generation (SHG) of N-methyl urea doped benzimidazole single crystal grown by VBT, J. Mater. Sci. Eng. A 3 (12) (2013) 806–813.
[15] G. Peramaiyan, P. Pandi, R.M. Kumar, Bulk growth, optical, thermal, dielectric and mechanical studies of nonlinear optical crystal, J. Therm. Anal. Calorim. 119 (1) (2015) 291–299.
[16] A. Krishna, N. Vijayan, C. Bagdia, K. Thukral, D. Haranath, K. Maurya, G. Bhagavannarayana, et al. Effect of ampoule support on the growth of organic benzimidazole single crystals by vertical Bridgman technique for nonlinear optical applications, Cryst. Eng. Comm. 18 (2016) 4844–4850.
[17] P.A. Praveen, S. Prabhakaran, R. Ramesh Babu, K. Sethuraman, K. Ramamurthi, Low power optical limiting studies on nanocrystalline benzimidazole thin films prepared by modified liquid phase growth technique, Bull. Mater. Sci. 38 (3) (2015) 645–651.
[18] P.A. Praveen, R. Ramesh Babu, K. Ramamurthi, Effect of substituents on polarizability and hyperpolarizability values of benzimidazole metal complexes, AIP Conf. Proc. 1731 (1) (2016) 090013.
[19] P.A. Praveen, R. Ramesh Babu, K. Ramamurthi, Linear and nonlinear optical properties of Mn doped benzimidazole thin films, AIP Conf. Proc. 1591 (1) (2014) 991.
[20] K. Chopra, Thin Film Device Applications, Springer Science & Business Media. 2012.
[21] E. Şahin, S. Ide, M. Kurt, Ş. Yurdakul, Structural investigation of dibromobis (benzimidazole) Zn(II) complex, J. Mol. Struct. 616 (1) (2002) 259–264.
[22] Ş. Yurdakul, M. Kurt, Vibrational spectroscopic studies of metal (II) halide benzimidazole, J. Mol. Struct. 650 (1) (2003) 181–190.

[23] H. Chang, M. Fu, X.-J. Zhao, E.-C. Yang, Four benzimidazole-based Zn(II)/Cd(II) polymers extended by aromatic polycarboxylate coligands: synthesis, structure, and luminescence, J. Coord. Chem. 63 (20) (2010) 3551–3564.
[24] W.-H. Sun, C. Shao, Y. Chen, H. Hu, R.A. Sheldon, H. Wang, X. Leng, X. Jin, Controllable supramolecular assembly by $\pi - \pi$ interactions: cobalt(II) and copper(II) complexes with benzimidazole derivatives, Organometallics 21 (21) (2002) 4350–4355.
[25] K. Singh, M.S. Barwa, P. Tyagi, Synthesis and characterization of cobalt(II), nickel(II), copper(II) and zinc(II) complexes with Schiff base derived from 4-amino-3-mercapto-6-methyl-5-oxo-1, 2, 4-triazine, Eur. J. Med. Chem. 42 (3) (2007) 394–402.
[26] U.P. Chaudhuri, R. Shakya, J.M. McClain, E.L. Klein, D.R. Powell, A. Grohmann, R.P. Houser, Copper(II), iron(II), and manganese(II) complexes of 2-methyl-2-(2-pyridinyl)-1, 3-propanediamine, Polyhedron 54 (2013) 84–90.
[27] S. Belaid, A. Landreau, S. Djebbar, O. Benali-Baitich, G. Bouet, J.-P. Bouchara, Synthesis, characterization and antifungal activity of a series of manganese(II) and copper(II) complexes with ligands derived from reduced N, N-O-phenylenebis (salicylideneimine), J. Inorg. Biochem. 102 (1) (2008) 63–69.
[28] J.J. Stewart, MOPAC: a semiempirical molecular orbital program, J. Comput. Aided Mol. Des. 4 (1) (1990) 1–103.
[29] Z.A. Fekete, E.A. Hoffmann, T. Körtvélyesi, B. Penke, Harmonic vibrational frequency scaling factors for the new NDDO Hamiltonians: RM1 and PM6, Mol. Phys. 105 (19-22) (2007) 2597–2605.
[30] M.C. Goh, D. Juhue, O.M. Leung, Y. Wang, M.A. Winnik, Annealing effects on the surface structure of latex films studied by atomic force microscopy, Langmuir 9 (5) (1993) 1319–1322.
[31] L.H. Dubois, R.G. Nuzzo, Synthesis, structure, and properties of model organic surfaces, Annu. Rev. Phys. Chem. 43 (1) (1992) 437–463.
[32] F. Chen, J. Goodfellow, S. Liu, I. Grinberg, M.C. Hoffmann, A.R. Damodaran, Y. Zhu, P. Zalden, X. Zhang, I. Takeuchi, Ultrafast terahertz gating of the polarization and giant nonlinear optical response in $BiFeO_3$ thin films, Adv. Mater. 27 (41) (2015) 6371–6375.
[33] P.C. Ray, Size and shape dependent second order nonlinear optical properties of nanomaterials and their application in biological and chemical sensing, Chem. Rev. 110 (9) (2010) 5332–5365.
[34] H. Manaa, A. Al Mulla, S. Makhseed, M. Al-sawah, J. Samuel, Fluorescence and nonlinear optical properties of non-aggregating hexadeca-substituted phthalocyanine, Opt. Mater. 32 (1) (2009) 108–114.
[35] W. Guo, X. Sun, J. Sun, X. Wang, G. Zhang, Q. Ren, D. Xu, Nonlinear optical absorption of a metal dithiolene complex irradiated by different laser pulses at near-infrared wavelengths, Chem. Phys. Lett. 435 (1) (2007) 65–68.
[36] H. Manaa, A. Tuhl, J. Samuel, A. Al-Mulla, N. Al-Awadi, S. Makhseed, Photophysical and nonlinear optical properties of zincphthalocyanines with peripheral substitutions, Opt. Commun. 284 (1) (2011) 450–454.
[37] S. Mathews, S.C. Kumar, L. Giribabu, S.V. Rao, Nonlinear optical and optical limiting properties of phthalocyanines in solution and thin films of PMMA at 633 nm studied using a cw laser, Mater. Lett. 61 (2007) 4426–4431.
[38] M. Saravanan, T.C. Sabari Girisun, G. Vinitha, S. Venugopal Rao, Improved third-order optical nonlinearity and optical limiting behaviour of (nanospindle and nanosphere) zinc ferrite decorated reduced graphene oxide under continuous and ultrafast laser excitation, RSC Adv. 6 (2016) 91083–91092.
[39] M. Razvi, A.H. Bakry, S. Afzal, S.A. Khan, A.M. Asiri, Synthesis, characterization and determination of third-order optical nonlinearity by cw z-scan technique of novel thiobarbituric acid derivative dyes, Mater. Lett. 144 (2015) 131–134.
[40] S. Zafar, Z.H. Khan, M.S. Khan, Study of self-defocusing, reverse saturable absorption and photoluminescence in anthraquinone PMMA nanocomposite film, Spectrochim. Acta A Mol. Biomol. Spectrosc. 118 (2014) 852–856.
[41] Purnima, D. Mohan, R. Dhar, Polarization-dependent Z-scan characterization for optical nonlinearity in pyran dye, Laser Phys. 23 (12) (2013) 125401.
[42] F. Moslehirad, M.H.M. Ara, M.J. Torkamany, Synthesis of composite Au/TiO_2 nanoparticles through pulsed laser ablation and study of their optical properties, Laser Phys. 23 (7) (2013) 075601.
[43] M.M. Ara, H. Naderi, A. Mobasheri, M. Rajabi, R. Malekfar, E. Koushki, Characterization and nonlinear optical properties of PVP/TiO_2 nano-fibers doping with Ag colloid nano-particles, Phys. E Low-dimensional Syst. Nanostruct. 48 (2013) 124–127.
[44] S. Alikhani, H. Tajalli, E. Koushki, Third order optical nonlinearity and diffraction pattern of Ni nanoparticles prepared by laser ablation, Opt. Commun. 286 (2013) 318–321.
[45] X. Tong, H. Zhang, D. Li, Effect of annealing treatment on mechanical properties of nanocrystalline α-iron: an atomistic study, Sci. Rep. 5 (2015) 8459
[46] W. Auwärter, D. Écija, F. Klappenberger, J.V. Barth, Porphyrins at interfaces, Nat. Chem. 7 (2) (2015) 105–120.
[47] A. Maxwell, A. Unwin, I. Ward, M.A. El Maaty, M. Shahin, R. Olley, D. Bassett, The effect of molecular weight on the deformation behaviour of pressure annealed polyethylene, J. Mater. Sci. 32 (3) (1997) 567–574.
[48] A. Zawadzka, P. Pciennik, J. Strzelecki, A. Korcala, A. Arof, B. Sahraoui, Impact of annealing process on stacking orientations and second order nonlinear optical properties of metallophthalocyanine thin films and nanostructures, Dyes Pigments 101 (2014) 212–220.
[49] G. Sreekumar, P.G.L. Frobel, C.I. Muneera, K. Sathiyamoorthy, C. Vijayan, C. Mukherjee, Saturable and reverse saturable absorption and nonlinear refraction in nanoclustered amido black dye polymer films under low power continuous wave HeNe laser light excitation, J. Opt. A Pure Appl. Opt. 11 (12) (2009) 125204.
[50] C. Dai-Jian, D. Sha, H. Jun-Bo, Z. Hui-Jun, X. Si, X. Gui-Guang, W. Qu-Quan, A sign alternation of nonlinear absorption in gold composite films in z-scan, Chin. Phys. Lett. 22 (9) (2005) 2286.
[51] P. Sharma, S. Roy, Effect of probe beam intensity on all-optical switching based on excited-state absorption, Opt. Mater. Express 2 (5) (2012) 548–565.